

# Dual-polarization radar and microwave radiometer observations of winter precipitation during LPVEx

Susanna Lautaportti<sup>1</sup>, Dmitri Moisseev<sup>1</sup>, Pablo Saavedra<sup>2</sup>, Alessandro Battaglia<sup>3</sup>, V. Chandrasekar<sup>1,4,5</sup>

<sup>1</sup>*University of Helsinki, P.O. Box 48, FIN-00014 Helsinki, Finland, susanna.lautaportti@helsinki.fi*

<sup>2</sup>*University of Bonn, 53121 Bonn, Germany*

<sup>3</sup>*University of Leicester, University Road, LE17RH, Leicester, UK*

<sup>4</sup>*Colorado State University, Fort Collins CO 80523-1373*

<sup>5</sup>*Finnish Meteorological Institute, P.O. Box 503, FIN-00101 Helsinki, Finland*

## 1. Introduction

In a number of published studies, radar observations of high differential reflectivity (Hogan et al. 2002, Moisseev et al. 2009, Andric et al. 2010) and specific differential phase (Kennedy and Rutledge 2011, Bechini et al. 2011) bands in winter storms and ice clouds were reported. Dual-polarization radar signatures in the bands can be explained by the scattering of radio waves by oblate, dense ice particles, i.e. pristine ice crystals. Just below those bands differential values smaller than 1 dB are observed. Those smaller values are typical for low density ice particles, such as aggregates. The bands typically occur at altitudes where temperatures are roughly  $-15^{\circ}\text{C}$ . There are several reports of the bands occurring at warmer temperatures around  $-4^{\circ}\text{C}$ , as well (Moisseev et al., 2009). While enhanced  $K_{DP}$  signatures are mainly observed inside precipitating clouds, high  $Z_{DR}$  values were observed both at cloud tops as well as inside of clouds.

The main explanation for those bands is that they are caused by the scattering of radio waves from ice crystals rapidly growing in presence of supercooled water. After reaching a certain size those crystals aggregate and the smaller differential reflectivity values are caused by snowflakes. This explanation is very plausible, however, it is not very clear how it is possible to observe differential reflectivity bands especially when they are embedded inside precipitating clouds. Because radar observations are much more sensitive to larger particles and a small number of aggregates should dominate the scattering, even if there are many more ice crystals present in an observation volume (Bader et al. 1987). Hogan et al. (2002) have shown that  $Z_{DR}$  bands occur in the areas where supercooled water is present, but there are no such observations corresponding to the  $K_{DP}$  bands. Since  $K_{DP}$  and  $Z_{DR}$  bands do not always occur at the same areas, question arises whether there is any difference in the physical cause of those bands and if so what it is. What role, if any, does supercooled liquid water play in forming  $K_{DP}$  bands?

During the Light Precipitation Validation Experiment (LPVEx, <http://lpvex.atmos.colostate.edu/>) that took place in Helsinki in fall 2010, we have collected a large number of observations of winter storms with the differential reflectivity and specific differential phase bands. In several cases the bands formed at altitudes lower than 1 km and extended to the ground. In this study we are focusing on the  $K_{DP}$  and the  $Z_{DR}$  bands observed in ten events at ground level. We analyze these events by using particle size distributions (PSDs) measurements carried out by a particle video imager (PVI). Furthermore, we study the presence of supercooled liquid water in  $K_{DP}$  and  $Z_{DR}$  bands by using liquid water path (LWP) values measured by a passive microwave radiometer, ADMIRARI.

## 2. Measurement setup

During the LPVEx we have collected a large number of observations of winter storms by using both in situ and remote sensing measurements. The radar measurements were carried out by using the University of Helsinki Kumpula radar (KUM). The KUM radar is a C-band dual-polarization weather radar located at the top of the Department of Physics building ( $60^{\circ}12.26'$  N,  $24^{\circ}57.78'$  E). The radar is positioned 59 m above the mean sea level and 30 m above the ground level.

A particle video imager (PVI) was used to record precipitating particle images. PVI is an imaging system which includes a video system (camera and lens), a lamp and a data logger. The video system is located 3 m from the camera and the focal plane is 2 m from the video system. This setup system minimizes the impact of wind to the recorded data. (Newman et al. 2009). From those images particle size distributions were calculated. The PVI was located at the University of Helsinki precipitation measurement site in the city of Järvenpää, 32 km north of the Kumpula campus.

Measurements collected by a multi-frequency passive microwave radiometer (ADMIRARI, ADvanced MICrowave RAdiometer for Rain Identification), provided by the University of Bonn for the experiment, was used to estimate liquid water paths (LWP) for the snow fall events presented in this study. The ADMIRARI has been designed to investigate precipitation processes. It comprises of six channels covering three frequencies (10.65, 21.0 and 36.5 GHz) and both linear polarizations (H and V) and it is intended for retrieving simultaneously water vapor, rain, and cloud liquid water paths (Battaglia et al. 2010). More detailed description about the ADMIRARI is presented in Battaglia et al. (2009). During our study period the ADMIRARI was pointing at a fixed  $30^{\circ}$  elevation angle towards the KUM radar. ADMIRARI was deployed in the backyard of the Vaisala head quarters, 10 km away from the Kumpula radar.

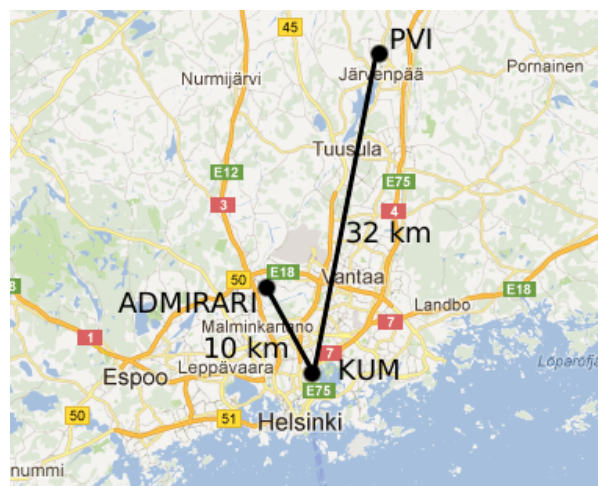


Fig. 1 The map of the measurement setup (Helsinki-Järvenpää Map 2012). The KUM radar is located in Helsinki, the PVI is located in Järvenpää and the ADMIRARI is located in Vantaa. The distance between the KUM radar and the PVI is 32 km and the distance between the KUM radar and the ADMIRARI is 10 km.

During the experiment, the KUM radar was performing RHI scans in the direction of the ADMIRARI and Järvenpää every 5 min. Both scans recorded the  $Z$ ,  $Z_{DR}$  and  $K_{DP}$ . For retrieving the  $K_{DP}$ , the algorithm developed by Wang and Chandrasekar (2009) is used. The locations of the instruments on the map of the Helsinki region are shown in Fig. 1.

### 3. Results

From the observations collected during the LPVEx we have identified more than 40 distinct snowfall events between September 15<sup>th</sup> and December 31<sup>st</sup> 2010. In this paper we are focusing on the snowfall events which occurred in December 2010. According to the KUM RHI scans towards the ADMIRARI we have a total of 3800 RHI scans which indicate precipitation at the ADMIRARI site (at least 2 sequential scans indicate continuous weather echo in the lowest 500m region above the ADMIRARI) which is 47% of all the RHI scans towards the ADMIRARI during December 2010. 48% of these RHI scans which indicate weather echo show also large  $Z_{DR}$  values ( $Z_{DR} > 2$  dB) above the ADMIRARI and 6% of weather echo scans indicate increased  $K_{DP}$  values ( $K_{DP} > 0.1$  deg/km). 3% of all the weather echo RHI scans have both a large  $Z_{DR}$  value and an increased  $K_{DP}$  value. According to the ground observations at the PVI location in Järvenpää and the atmospheric soundings performed in Jokioinen (approximately 95 km to north-west from the ADMIRARI location) the temperature throughout the whole atmosphere was constantly below 0°C in December 2010.

#### 3.1 KUM & ADMIRARI

The LWP values were calculated from the ADMIRARI measurements using the method described by Löhnert and Crewell (2003). It should be noted that the smallest detectable LWP value by ADMIRARI is 30g/m<sup>2</sup>. By applying this value as a threshold it was found that 79% of the analyzed precipitation cases indicate presence of supercooled liquid water. The LWP values are ranging from 30 to 625 g/m<sup>2</sup>.

Fig. 2 shows the LWP values in the precipitation cases during December 2010. Fig. 2a presents LWP observations for all the precipitation cases in December 2010. In Fig. 2b-d LWP observations corresponding to the high  $Z_{DR}$  cases are shown and in Fig. 2f-h the cases where detectable  $K_{DP}$  values ( $K_{DP} > 0.1$  deg/km) are depicted. Fig 2e represents the cases which consist of both high  $Z_{DR}$  and detectable  $K_{DP}$  values. The red dots represent the precipitation cases where the LWP value is below the threshold value (30 g/m<sup>2</sup>). For calculating the average LWP value (indicated by black line in each figure) we assume that these cases do not have any liquid water present, i.e. LWP = 0 g/m<sup>2</sup>.

From figure 2 we can infer the overall trend that the average LWP value decreases as  $Z_{DR}$  increases. This decrease, however, is not very large. Furthermore, even though there is a lot of variability between the cases, the general trend is that there are fewer high LWP observations as  $Z_{DR}$  increases. These observations are in agreement with the water vapor deposition growth of ice crystals in presence of super cooled liquid water. Higher  $Z_{DR}$  values imply larger crystals, that have depleted water resources as they grow.

The LWP observations for the  $K_{DP}$  cases are shown in Fig. 2 (f-h). One can observe that  $K_{DP}$  cases have lower LWP values if compared to the pure  $Z_{DR}$  cases. Furthermore, the highest  $K_{DP}$  cases show almost negligible LWP values. These observations imply that high  $K_{DP}$  values are observed when the super cooled liquid water is almost depleted by crystal growth. Therefore in those cases the vapor deposition crystal growth is not the dominating growth mechanism, and probably aggregation is the main process responsible for snowflake growth. As the aggregation starts the number of ice crystals becomes smaller, which in turn should reduce the  $K_{DP}$ . This, however, is not observed.

#### 3.2 KUM & PVI

In December 2010 the KUM radar RHI scans show ten separate cases where either an increased  $K_{DP}$  or a high  $Z_{DR}$  areas touches the ground at the PVI location. Two of the cases have detectable  $K_{DP}$  values (see example in Fig. 3a), four of the cases have high  $Z_{DR}$  values (see example in Fig. 3b) and four of the cases have both high  $Z_{DR}$  and detectable  $K_{DP}$  values. Figure 4 shows average normalized PSD for all cases. The  $N(D)$  is measured by the PVI where the  $D$  indicates the largest

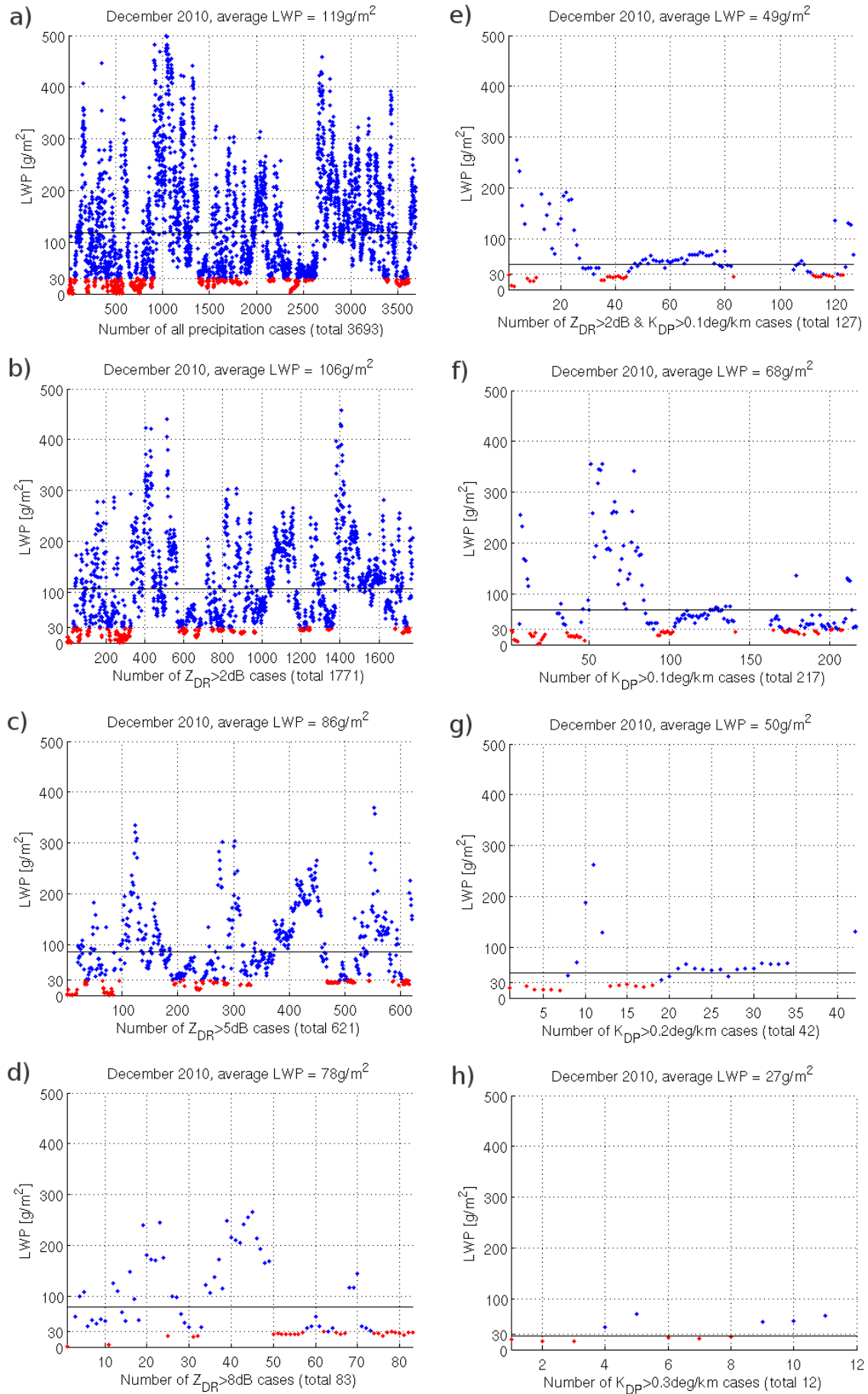


Fig. 2 The LWP values (blue dots) in (a) all precipitation cases, (b-d) high Z<sub>DR</sub> cases, (e) combined Z<sub>DR</sub> and K<sub>DP</sub> cases and (f-h) increased K<sub>DP</sub> cases. The red dots indicate LWP < 30g/m<sup>2</sup> cases. The black line indicates the average LWP value of each represented cases.

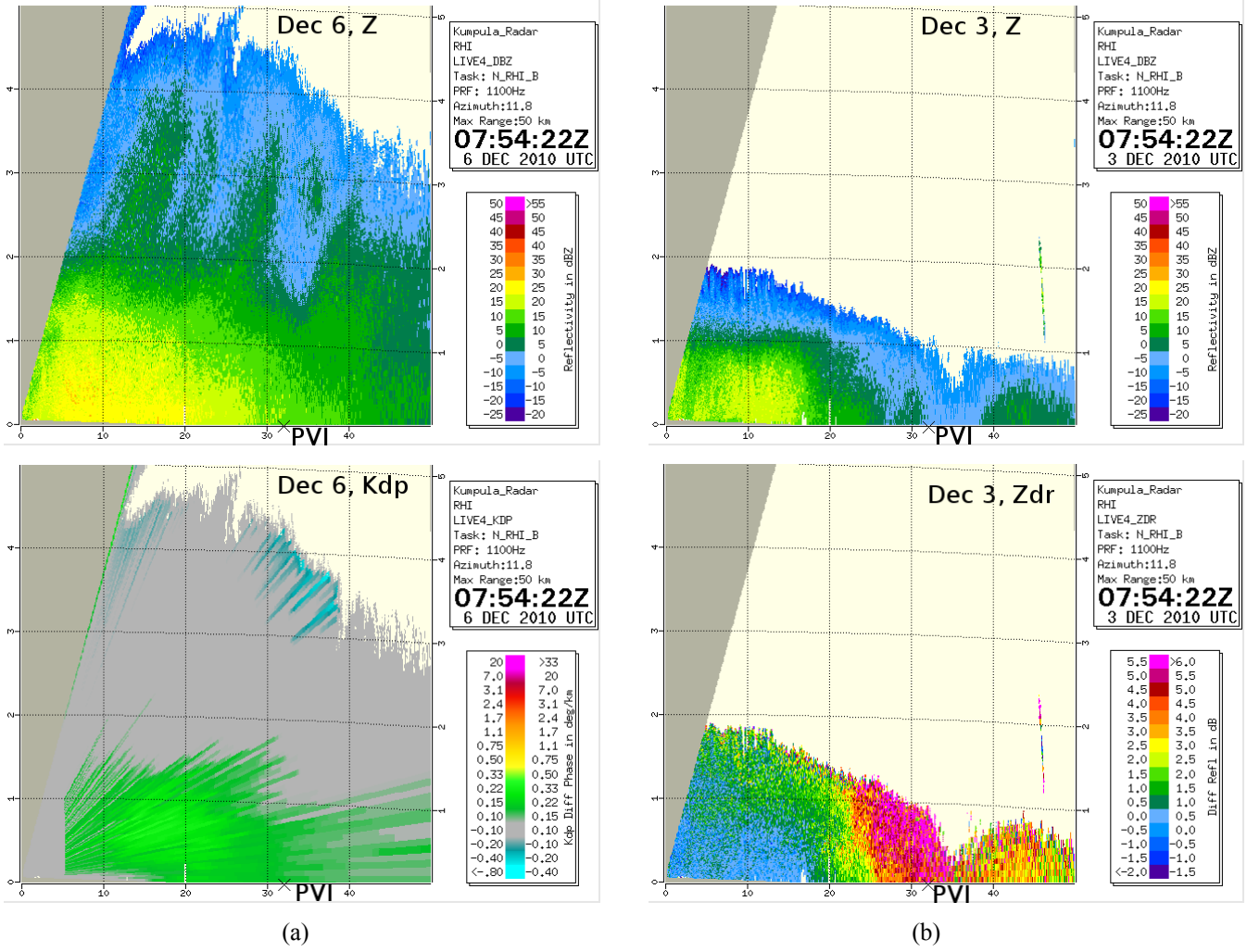


Fig. 3 Examples of a  $K_{DP}$  case (column a) and a  $Z_{DR}$  case (column b).

width of the particle. Particle size distributions are normalized by the intercept parameter,  $N_0$ , and  $D$  by the median volume diameter,  $D_0$ . Those parameters are determined by assuming the exponential PSD

$$N(D) = N_0 \exp(-AD) \quad (1a)$$

where

$$A = \frac{3.67}{D_0} \quad (1b)$$

$$N_0 = N_t * A \quad (1c)$$

and  $N_t$  is calculated by integrating the observed PSD.

The overall shapes are very similar and it is difficult to discriminate between events based on the normalized PSD only. The situation changes when we start considering  $N_0$  normalized reflectivity and  $K_{DP}$  observations as a function of  $\Lambda$ , where the radar observables are taken from KUM RHI scans. In Fig. 5 those observations are shown. It can be seen that both the normalized reflectivity factor and  $K_{DP}$  increase as  $\Lambda$  decreases. The decrease of  $\Lambda$  is generally associated with progression of the aggregation growth of snowflakes (Lo and Passarelli 1982). They have reported that the minimum observed  $\Lambda$  is about  $10 \text{ cm}^{-1}$ .

In Fig. 5 a,b the plus symbols correspond to the  $Z_e$  and  $K_{DP}$  values observed by the radar. In Fig. 5a the black curve depicts modeled  $Z_e$  values and the red curve is the best fit to the modeled data. In Fig. 5b the red curve is representing the best fit to the observations. Based on the modeling and fitting, the relations between normalized radar observables and  $\Lambda$  can be inferred:

$$\frac{Z_e}{N_0} = 0.02 A^{2(1-\log_{10}(A))} \quad (2)$$

$$\frac{K_{DP}}{N_0} = 1.24 A^{-3.4} \quad (3)$$

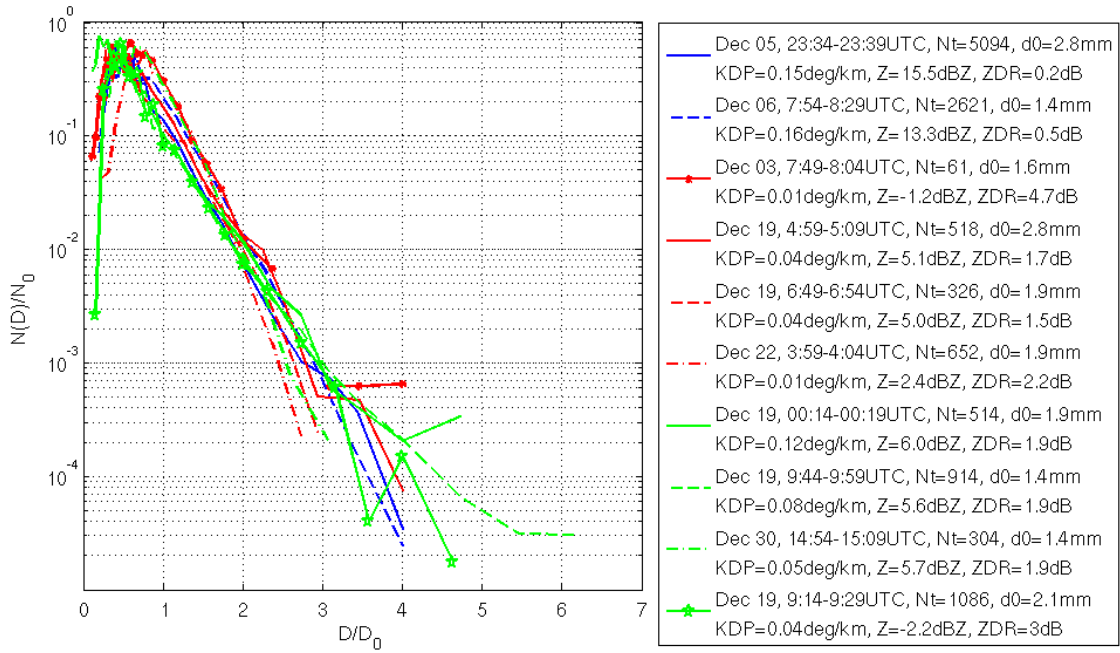


Fig. 4 Normalized PSDs. Blue indicates  $K_{DP}$  cases, red indicates  $Z_{DR}$  cases and green indicates combined  $Z_{DR}$  and  $K_{DP}$  cases.

In this study the modeling of the equivalent reflectivity factor,  $Z_e$ , for each measured PSD was done as follows (Bringi and Chandrasekar 2001):

$$Z_e = \frac{|K_{ice}|^2}{|K_w|^2} \int \rho(D)^2 D^6 N(D) dD \quad (4)$$

where  $N(D)$  was assumed to be the exponential distribution (1) and for  $N_0$  and  $\Lambda$  we used the values calculated from the PVI measurements. For determining the density  $\rho(D)$  we modeled snow particles as oblate spheroids with an aspect ratio of 0.6 (Korolev and Isaac 2003) and mass-size relations as :

$$m = a_1 D^2, D \leq 0.2 \text{ cm} \quad (5a)$$

$$m = a_2 D^{2.5}, D > 0.2 \text{ cm} \quad (5b)$$

the  $a_1$  and  $a_2$  terms were found by optimizing the fit of the model (4) to the observed  $Z_e/N_0 - \Lambda$  observations. The obtained mass-diameter relations, in cgs units, are the following:

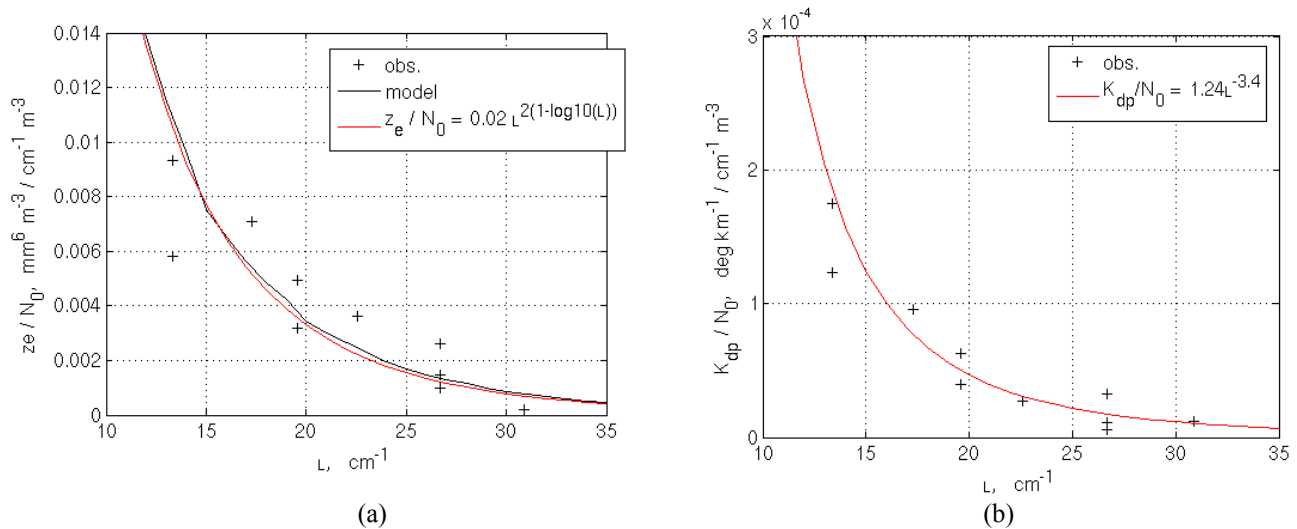


Fig. 5 (a)  $Z_e/N_0 \sim \Lambda$  and (b)  $K_{DP}/N_0 \sim \Lambda$  relations. + indicates the values observed by the KUM radar for each separate case (shown in Fig. 4). In 4a the black curve represents the modeled values and the red curve is the best fit for the modeled values. In 4b the red curve is the best fit for the observed values.

$$m=0.008D^2, D \leq 0.2 \text{ cm} \quad (6a)$$

$$m=0.002D^{2.5}, D > 0.2 \text{ cm} \quad (6b)$$

The relations (6 a-b) indicate there are two types of particles present in the volume, smaller particles are more dense than the larger ones. In this study we have not attempted to model both  $Z_e$  and  $K_{DP}$  observations, as a result the modeled axis ratios are assumed to be 0.6 for all particle sizes.

#### 4. Conclusions

From this study we have learned that  $Z_{DR}$  and  $K_{DP}$  bands are observed in different conditions. Liquid water paths for the high  $Z_{DR}$  cases are generally larger than ones for the  $K_{DP}$  cases. Unfortunately, radiometer observations give only column integrated observations. Therefore, we have to speculate that observed supercooled liquid water signatures are associated with the bands. Regardless of this, we can reason that whatever mechanism is responsible for the high  $K_{DP}$  cases, it does not require large amounts of supercooled water. Therefore, we argue that vapor deposition growth of ice crystals is not important in those cases. Since the aggregation would deplete the number of ice crystals, some other mechanism should be responsible for the creation of oblate dense particles, responsible for the  $K_{DP}$  signatures. Moisseev et al. (2012) shows that the aggregation process produces small aggregates. The formation of these “aggregate embryos” can happen without supercooled liquid water. The aggregate embryos are very oblate and cause large  $K_{DP}$  values. The imagery taken by the PVI, not shown in this paper, has shown that these aggregate embryos exist in the increased  $K_{DP}$  areas. This indicates that the high  $K_{DP}$  area is a natural manifestation of the aggregation process.

If our above stated conclusion that enhanced  $K_{DP}$  signatures are a natural manifestation of the aggregation process is correct the found relations (2-3) between normalized  $K_{DP}$  and  $Z_e$  show a promise of using dual-polarization observations for retrieval of PSD parameters in natural snowfall and eventually in improved QPE. Analysis of more cases is needed to give a definitive answer.

#### References

- Andric J., Zrnica D., Straka J., Melnikov V., 2010: The enhanced  $Z_{DR}$  signature in stratiform clouds above melting layer. Preprints, *13<sup>th</sup> Conf. On Cloud Physics*, Portland, OR, Amer. Meteor. Soc., P2.89. [Available online at <http://ams.confex.com/ams/pdfpapers/171308.pdf>.]
- Bader M. J., Clough S. A., Cox G. P., 1987: Aircraft and dual polarization observations of hydrometeors in light stratiform precipitation. *Quart. J. Roy. Meteor. Soc.*, **113**, 491–515
- Battaglia A., Saavedra P., Rose T., Simmer C., 2009: Rain observations by a multi-frequency dual polarized radiometer. *IEEE Geosci. Remote Sens. Lett.*, **6**, 354–358.
- Battaglia A., Saavedra P., Rose T., Simmer C., 2010: Characterization of Precipitating Clouds by Ground-Based Measurements with the Triple-Frequency Polarized Microwave Radiometer ADMIRARI. *J. Appl. Meteor.*, **49**, 394–414
- Bechini R., Baldini L., Chandrasekar V., Cremonini R., Gorgucci E., 2011: Observations of Kdp in the ice region of precipitating clouds at X-band and C-band radar frequencies. Preprints, *35<sup>th</sup> Conf. on Radar Meteor.*, Pittsburg, PA. Amer. Meteor. Soc., 7A.4. [Available online at [http://ams.confex.com/ams/35Radar/webprogram/Manuscript/Paper191528/kdp\\_ice\\_ams\\_extabstractLB\\_letter.pdf](http://ams.confex.com/ams/35Radar/webprogram/Manuscript/Paper191528/kdp_ice_ams_extabstractLB_letter.pdf)]
- Bringi V. N., Chandrasekar V., 2001: *Polarimetric Doppler Weather Radar: Principles and Applications*. Cambridge University Press, 636 pp.
- Helsinki-Järvenpää Map, 2012, Scale undetermined, using 'Google Maps', <http://maps.google.com/>, 24 May 2012.
- Hogan R. J., Field P.R., Illingworth A. J., Cotton R. J., Choullarton T. W., 2002: Properties of embedded convection in warm-frontal mixed-phase cloud from aircraft and polarimetric radar. *Quart. J. Roy. Meteor. Soc.*, **128**, 451–476
- Kennedy P. C., Rutledge S. A., 2011: S-band dual-polarization radar observations of winter storms. *J. Appl. Meteor.*, **50**, 844 – 858
- Korolev A., Isaac G., 2003: Roundness and aspect ratio of particles in ice clouds. *J. Atmos. Sci.*, **59**, 1795–1808
- Lo K. K., Passarelli R. E. Jr., 1982: The growth of snow in winter storms: An airborne observational study. *J. Atmos. Sci.*, **39**, 697–706.
- Löhnert, U., Crewell S., 2003: Accuracy of cloud liquid water path from ground-based microwave radiometry 1. Dependency on cloud model statistics, *Radio Sci.*, **38**, 8041, doi:10.1029/2002RS002654.
- Moisseev, D., E. Saltikov, and M. Leskinen, 2009: Dual-polarization weather radar observations of snow growth processes. Preprints, *34<sup>th</sup> Conf. on Radar Meteorology*, Williamsburg, VA, Amer. Meteor. Soc., 13B.2. [Available online at <http://ams.confex.com/ams/pdfpapers/156123.pdf>.]
- Moisseev, D., Lautaportti S., Bliven L., Chandrasekar V., Kulmala M., 2012: Aggregation growth of snowflakes observed by radar and ground based particle video imager. *16<sup>th</sup> International Conference on Clouds and Precipitation*, Leipzig, Germany
- Newman A. J., Kucera P. A., Bliven L. F., 2009: Presenting the snowflake video imager (SVI). *J. Atmos. Oceanic Technol.*, **26**, 167–179
- Wang Y., Chandrasekar V., 2009: Algorithm for estimation of the specific differential phase. *J. Atmos. Oceanic Technol.*, **26**, 2565–2578